A Novel Procedure for the Topology Optimization of an Engine Exhaust Mixer

Federico Colombo [1], Vincenzo Vitiello [4], Flavio Cimolin [2], Luca Patricelli [1], Alberto Guardone [3]

[1] Leonardo S.p.A. Helicopters Division
[2] Siemens S.p.A.
[3] Politecnico di Milano
[4] Akka Technologies

Abstract: The design of the engine primary exhaust of a helicopter must guarantee that the backpressure induced at the turbine outlet is sufficiently low to expel the hot air from the vehicle without compromising engine performances. At the same time, a large enough mass flow of air from the engine bay (secondary flow) is imposed to properly ventilate the bay. To this purpose, the exhaust is composed of two parts: the primary exhaust which conveys the air flow from the engine outlet and the secondary flow which collects the air from the primary exhaust and the air from the engine bay. The exhaust is designed with the aim of minimizing the backpressure at the engine outlet (minimizing therefore the fuel consumption) and of providing a secondary flow to properly ventilate the engine bay. In this paper, the discrete adjoint of the compressible Navier-Stokes equations coupled with the level-set method for the topology optimization is applied to this complex aerodynamic scenario, with the aim of designing a geometry able to minimize the impact on engine fuel consumption while fulfilling all other design requirements. The design case analyzed is the primary exhaust of the tilt-rotor demonstrator developed by Leonardo Helicopter division within the Clean Sky 2 Fast RotorCraft framework. Since the topologic optimization has been only recently introduced in Computational Fluid Dynamics tool, this work duly investigate all the steps required for the optimization. These include the choice of the constraints and the analysis of the error introduced by the Brinkman Penalization Model, which is used to simulate the solid domain introduced in the fluid field including some detail on modelling the walls generated by the optimization process. The impacts of the developed solutions are at the end compared with the primary exhaust developed using standard methodologies. Two novel geometries are produced which fulfill all design requirements. All simulations were performed using Siemens PLM commercial software STAR-CCM+.

Keywords: Topology optimization, Brinkman Penalization Model, Tilt rotor, Level-Set Methods, Sensitivity Analysis, Discrete Adjoint

1. Introduction

Topology optimization originates in the structural and solid mechanics field as an alternative to shape and sizing optimizations. The basic concepts of this technique were posed by Bendsøe and Kikuchi [1] in the late 1980s with the introduction of a homogenization method. Topology optimization poses itself as a material distribution technique that, in its structural formulation, aims to find the optimal distribution that can improve the performance of a structural component under specific constraints; in other words, topology optimization aims to give an answer to the question “where should solid material be placed?” or, alternatively, “where should the holes be inserted?" [2]. The greatest advantage introduced by this methodology lies in the fact that there is no need for a predefined shape, but only for the available design space in which the desired component shall lie. As a consequence of this, two other characteristic of this methodology have contributed to its development: the first, obviously, lies in the simplified identification of the best material distribution for satisfying the various constraints introduced optimizing the objective function. The second resides in the lower amount of time required: through the topological optimization it is in fact possible to obtain the best form in a very short amount of time, avoiding other longer methodologies such as the procedures of trial and error or those based on experiences of the designer.

One the other way, one of the main problem introduced by this methodology lies in the fact that the geometry obtained in this way is somehow "natural" and, therefore, difficult to replicate with the standard methodologies of CAD design and manufacturing. An aid to the development and application of this technology comes from the parallel development of Additive Manufacturing technologies, which have greatly expanded the production capabilities of more complex shapes and geometries and have opened up the possibility of generating and testing geometries obtained from topological optimization as they are and not a simplified replica of them, but which is still undergoing studies and certifications processes for the aeronautical applications [3] [4].

The basic idea of the original methodology is applicable to all those physics in which the governing equations can be described by a set of partial differential equations (PDEs), which therefore enlarges its applications to a high variety of different physics such as acoustics, electromagnetism, heat conduction, fluid flow, etc. [5].

It is in the latter field that the work of this article is developed: when applied to a fluid field, the above question should be changed in “where should the fluid flow?”. Although the basic concepts behind the development of material within the physical domain is the same of the one used in structural optimization, the presence of a solid portion of material in a complex field such as the fluid-dynamics one introduces some limitations and issues to the development of the flow: the simulation of a solid domain inside a fluid field must indeed be able to replicate the effects that it have on the flow field, not only in terms of not passage of fluid, but also and above all in terms of development of the boundary layer and turbulence. These issues are still present in the models used for the implementation of this optimization methodology, thus limiting considerably the applications: most of them are in fact related to the study of the optimal geometry of ducts or piping systems for the reduction of pressure drops or for guaranteeing uniformity to an outlet flow, but it cannot go beyond these applications.

The present work regards the investigation of these issues and aspects, acquiring notions on the physical limits introduced by the optimization models currently developed and some possible correction to them, with the aim of make this promising technology as innovative feature for the design of some critical components. All the analyses were performed on Siemens STAR-CCM+ [6], which in the release v2020.3 (September 2021) firstly introduced the possibility of performing fluid-dynamic topology optimization based on the Brinkman Penalization Model [7] later on described. Since it is a brand-new physical model inside this software, the work here proposed was “divided” in two different sections: in the first part an analysis of the model, its performances and limitations are analyzed and a procedure for its application and improvement is developed and presented. In the second part the latter is applied to a case of interest to analyze its capability on a complex aerodynamic scenario: in particular, this work focused on the primary exhaust of the GE CT7-2E1 engine of a tilt rotor technology demonstrator, under development in the framework of EU Horizon 2020 Clean Sky 2 [8]. The tilt rotor is the Next Generation Civil Tilt Rotor Technology Demonstrator (NGCTR-TD) [9], developed by the Work Area Leader (WAL) Leonardo Helicopters, which is planned to perform the first flight tests in 2023. All activities have been developed within Clean Sky 2 Joint Undertaken project, which aims at studying and developing of new technologies for the aeronautical design process.

2. Topology optimization model and workflow

To understand how TO works and behave, it is necessary to firstly introduce some mathematical concepts that allow to focus on the main key points of the solid domain generation and characterization inside the fluid domain.

The general workflow of TO (**Figure 1**) consists of two main steps: the first one concerns the adjoint analysis, which is needed to define the solid domain, while the second one consist of solving the primal solution with the new solid domain inside the fluid one.

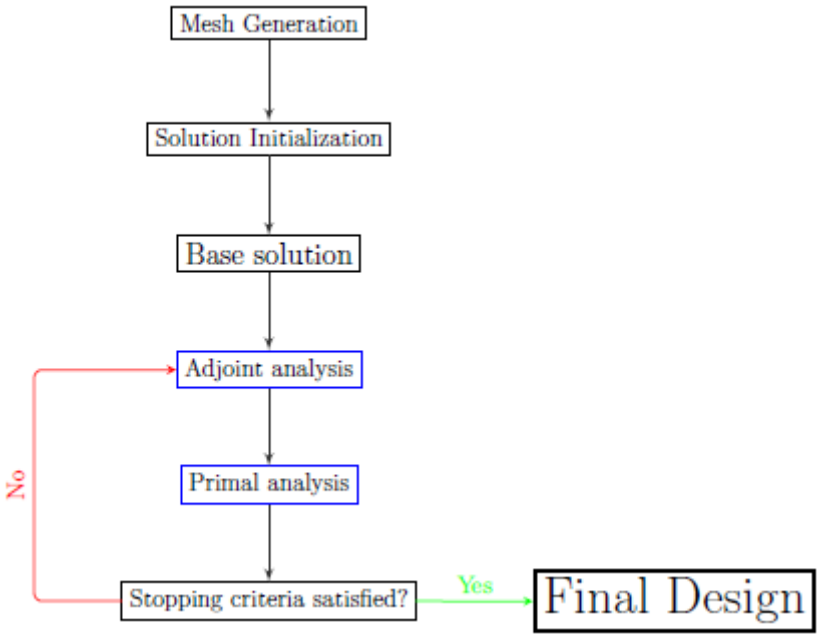

***Figure 1**: Generic Topology Optimization Workflow*

Nowadays, the two most common methods to define the solid region are:

- Density-based methods (SIMP) [1];
- Level-set methods (LSMs) [10] [11] [12].

The density-based approach is the most popular TO method, since it has a solid mathematical foundation, it can handle various constraints and objective functions and it is quite easy to implement in a FE environment. This method is also known as Solid Isotropic Material with Penalization (SIMP) and was originally proposed by Bendsoe and Kikuchi (1988). The idea behind the finite element based SIMP method is that it is possible to associate a pseudo-density variable ρ_e to every single element, called isotropic solid micro-structure, that allows to parameterize the topology, that can vary between a minimum value ρ_{min} (different from zero to avoid numerical problems) that identifies the empty domain, and 1, thus allowing the assignment of intermediate densities for the cells. The optimization aims to identify the best distribution of ρ_e that can minimize (or maximize) the objective function.

The other most common popular TO approach, used also for this work, are the Level-set Methods (LSMs), which define the interfaces between material phases implicitly using isolines of a Level-set Function (LSF). The LSF is used to describe the boundaries of a solid occupying the domain according to the following definition:

$$\emptyset(x,y) = \begin{cases} < 0, & if\,(x,y) \in \Omega \\ = 0, & if\,(x,y) \in \delta\Omega \\ > 0, & else \end{cases} \qquad \textit{(Eq. 1)}$$

Where (x,y) is any pont in the domain and Ω is the fluid domain.

The shape and the topology of the domain change during the optimization according to the Level set function, which evolves according to the following Hamilton- Jacobi transport equation:

$$\frac{\partial \phi}{\partial \tau} + V\nabla\phi = 0 \qquad \textit{(Eq. 2)}$$

where τ is a fictitious time parameter ($\tau > 0$) which allows to simulate the evolution of the LSF, while V is the interface velocity between two phases.

Unlike density-based ones, this kind of representation can create crisp interfaces between material phases avoiding ambiguities of intermediate material phases. To characterize a cell as solid or fluid, the idea behind SIMP method is then recalled, introducing a porosity function, called *Material Indicator function*, defined as:

$$\chi = 0.5 \cdot \left[1 - atan\left(\frac{\phi}{\delta}\right)\right] \qquad \textit{(Eq. 3)}$$

where $\delta \neq 0$ defines the interface dimension (usually $\delta = 0.1$).

The main task of an optimization problem is to maximize (or minimize) an objective function $f(x)$ while satisfying a series of constraints c_i. Instead of dealing with a constrained optimization, LSFs methods introduce the Lagrangian function *(Eq. 4)* which becomes the new objective function, generating an unconstrained optimization.

$$\mathcal{L}(x, \lambda) = f(x) + \sum \psi(c_i, \lambda_i^k, \mu) \qquad \textit{(Eq. 4)}$$

where λ_i are the Lagrange Multipliers and μ is the constraints' weight.

Inside STAR-CCM+ the optimization is performed via a Stochastic Gradient Descent [13].To increase the robustness of the optimization, the evolution of the LSF is governed by the interface velocity V which is obtained via the ADAM algorithm [14] as a function of the *sensitivity* of the Lagrangian w.r.t the material indicator function (*Eq. 5)* which involve the sensitivities of the objective function and of the constraints. In order to correctly compare them, since the constraints can be of a different physical quantity w.r.t $f(x)$ an adimensionalization is required; by now, the most common one is based on the greatest value of the sensitivity function itself, which aims to give to the adimensionalized function an indication of the *distance* from the constraint's limit *(Eq. 6)*.

$$V = V\left(\frac{d\mathcal{L}}{d\chi}\right) = V\left(\frac{df}{d\chi}, \frac{dc_i}{d\chi}\right) \qquad \textit{(Eq. 5)}$$

$$\hat{f}(x) = \frac{f(x)}{\frac{df}{d\chi}} \quad , \quad \hat{c_i} = \frac{c_i}{\frac{dc_i}{d\chi}} \qquad \textit{(Eq. 6)}$$

On the consequences of *(Eq. 6)* we will talk about later on, since the development of the solid domain strictly depends on how the sensitivities are compared to each other.

As stated before, the definition of the solid domain is only the first part in the TO workflow; it is indeed fundamental to model correctly its effect on the fluid field. The most established technique for simulating a solid inside a fluid domain is by assigning a small porosity to those cells identified through the LSF interface. By now, the simplest and most established model that is based on this property is the Brinkman Penalization model, which adds a source term in the momentum equation that forces the velocity to zero in those cells with a non-zero porosity (identified via the material indicator function):

$$\frac{\partial \rho \boldsymbol{v}}{\partial t} + \nabla \cdot (\rho \boldsymbol{v} \otimes \boldsymbol{v}) = \quad -\nabla \cdot \sigma - \alpha(1 - \chi)\boldsymbol{v} \qquad \textit{(Eq. 7)}$$

where α is the strength of such a source term, also called *Brinkman Penalization Magnitude*.

The greatest advantage of this model lies in its simplicity and in the non-need of other quantities w.r.t to the ones computed during the optimization and topology definition (which are highly-computational-cost operations). On the other hand, due to its simplicity, this model inherently carries with it some approximations; ideally, the solid material shall be completely impermeable for both convective mass transport and pressure diffusion: while the former is easily simulated by forcing the velocity to zero, the Brinkman approach cannot prevent the latter and thus may lead to errors in flow prediction [15] [16]. Furthermore, the interfaces between fluid and solid are not characterized as no-slip walls, leading to an incorrect boundary layer development and turbulence modeling [17].

3. Basic Model Performance Analysis and New Sensitivity Analysis

In order to analyze how the Topology Optimization model implemented inside STAR-CCM+ works and how fair is the Brinkman Penalization Model in modeling the effect of the new solid domain, some simple test cases have been studied, starting from a simple Quasi-2D mass flow splitting duct. The aim of this analysis was to identify the weaknesses of the model to introduce some corrections that would be able to increase the accuracy and the robustness of the analysis.

Since TO does not need a pre-defined geometry on which to work with, the domain of analysis (cfr. **Figure 2**) is made in such a way that it represents the whole available domain for the final solid geometry. The goal of the optimization is to find the best geometry that could guarantee an equal flow division between the two outlets (which are fixed and not alterable) with the lowest possible pressure losses of the system.

As stated before, the optimization process can be considered as made of two main steps, alternating with each other: the solid domain definition and the solid domain effect simulation. The tests performed on this case took into account some of the main parameters that can influence both of them, starting with the ones concerning the first one: τ and μ. While τ governs how fast the LSF evolve between two Primal Analysis, affecting therefore the convergence, μ (also called "Penalty") works on the definition of the interface velocity and so on the evolution of the LSF itself: the greater is the penalty value, the greater is the influence of the constraints.

Starting with the latter, five different values of μ were chosen: from 10 to 10000. From the results of the optimization, the importance and influence of the penalty is clearly visible: with low values (10 and 100) the constraints are hardly satisfied, while the objective function is the real driving force of the optimization. The final topology is indeed well performing from the objective function point of view, but the constraints are very far from being satisfied, since a greater satisfaction would lead to an increase on the objective function. This is a problem, since we do not want the lowest possible value of the objective function, but we need the lowest possible value according to the given constraints. With higher values (5000 and 10000) the constraints are quickly satisfied but the solution starts to oscillate and don't manage to converge to the optimal one: the objective function is not perceived correctly by the optimization while the constraints seems to plays a role only when they are violated, while once satisfied seems to be no longer considered. With the middle value, a coherent solution was actually obtained, even though a convergence cannot be fully reached: investigating some more values near the chosen one lead to a good convergence with a coherent analysis, but requiring a trial-and-error procedure.

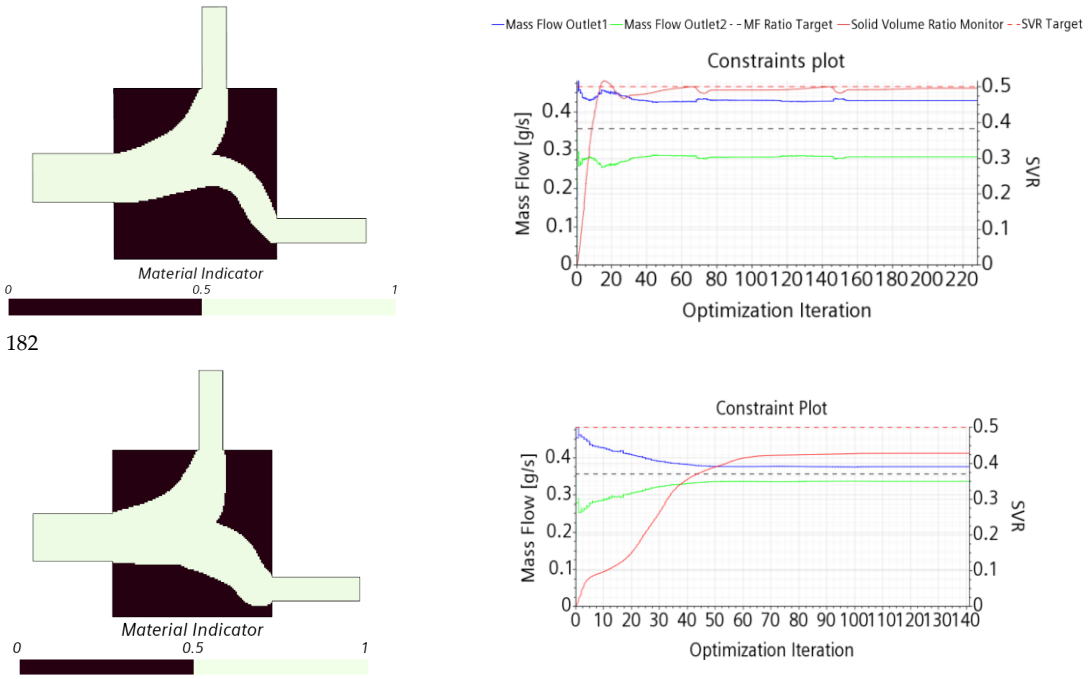

182

***Figure 2**: comparison between the analysis with a high penalty value (above) with the one with a low penalty value (below)*

Downstream of the results of the analysis on the Penalty parameter, it may come natural to wonder whether a different choice in the step size could reduce the oscillations generated in the cases with the highest value of Penalty. Since it has no physical meaning, it can be difficult to guess a good and consistent time step, so it can be useful to investigate the problems that can be generated when a wrong value is chosen. It is fundamental to understand that the choice of the step size also influences indirectly the interface velocity: the Adam algorithm aims to give it a "momentum" that tries to avoid the solution to stuck in local minima (or maxima); a too low value of the step size would generate a too low value of such a momentum, reducing the effectiveness of the ADAM algorithm.

Such reduction is indeed the only great effect that the solution experienced (**Figure 3**): while with higher values the oscillations around the optimum are slightly increased (as expected), reducing its value lead to a (stable) convergence to a local minimum, which is not the purpose of such a reduction.

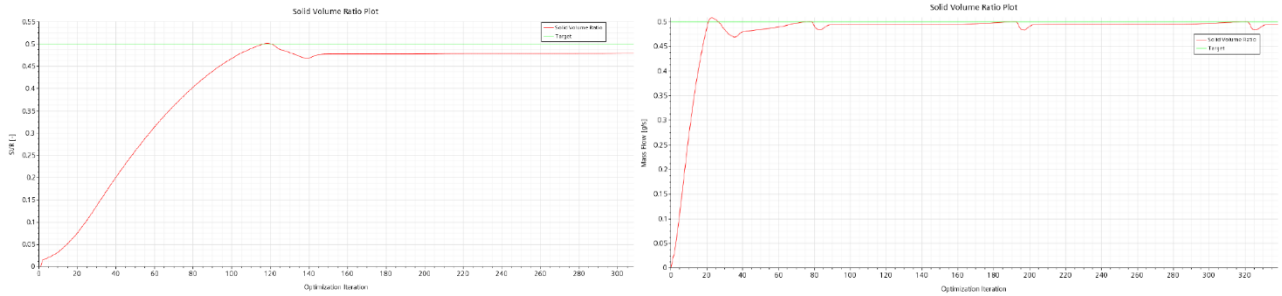

***Figure 3**: convergence plot with a low (left) and high (right) step size parameter.*

We can therefore state that the choice of the step size value is not as influencing as the one of the penalty parameter.

Analyzing the solution behavior and the development of the LSF as the optimization proceeds, it is clear what is the real driving force of the optimization itself: as described in (*Eq. 5*), the interface velocity is obtained from the sensitivity of the objective function and constraints w.r.t the material indicator function. A correct comparison between them is therefore crucial for the correct convergence of the LSF to the real optimum of the Lagrange function. By now, the sensitivities are compared thanks to an adimensionalization as per *(Eq. 6)*. A new adimensionalization was then introduced to guarantee the correct relationship between the objective function (which must be the driving force of the optimization) and the constraints.

For what concerns the objective function, in order to not introduce any new maxima or minima in the function itself, the adimensionalization is just made with an adimensionalizing coefficient and taken as reference for the constraints' one:

$$\tilde{f} = \frac{f}{\delta_f} \qquad \textit{(Eq. 8)}$$

The one concerning the constraints is based on a piecewise function which aims to distinguish between pre and post constraint satisfaction:

$$\tilde{c_i} = \begin{cases} \alpha_i \left(\dfrac{c_i - \overline{c_i}}{\delta_i}\right)^2, & c_i \leq \overline{c_i} \\ \beta_i \left(\dfrac{c_i - \overline{c_i}}{\delta_i}\right)^2, & c_i > \overline{c_i} \end{cases} \qquad \textit{(Eq. 9)}$$

where δ_i is the adimensionalizing coefficient, chosen accordingly with δ_f (ex. the order of magnitude) and α_i and β_i are the new weight of the constraints. The quadratic function is introduced to guarantee a continuous derivability of the adimensionalized constraints function $\tilde{c_i}$ in the neighborhood of $\overline{c_i}$. The constraint therefore becomes:

$$\tilde{c_i}|_{max} = 0 \ , \qquad \forall \ i \qquad \textit{(Eq. 10)}$$

The focus is then on the correct computation of the new weights: to guarantee the correct relationship between the sensitivity of the adimensionalized objective function with the ones of the adimensionalized constraints, α and β are computed as depicted in **Figure 4.** Based on the value of the sensitivity of $\tilde{f}$ at the beginning (convergence of the Base Solution with the basic geometry domain) and on the constraint satisfaction at the same iteration, a ration between the sensitivities is established and an initial value for α (if $c_i \leq \bar{c}_i$) (or β if $c_i > \bar{c}_i$) is guessed and the sensitivity of the constraint is computed. The ratio between the sensitivities is then computed and compared with the established one; the constraint's weight is therefore corrected and sensitivities recomputed. The loop is repeated until the correct ratio is obtained. The sensitivity ratio chosen shall not be a fixed number, but it is enough to guess an order of magnitude of such a ratio.

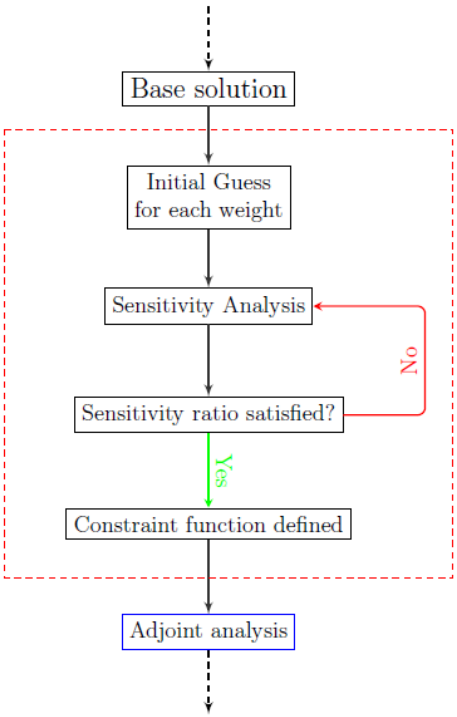

***Figure 4**: constraints' weight computation loop*

With such a definition of the adimensionalized functions, we can assure the following:

I. Faster and more stable convergence
II. Correct and coherent consideration of the constraints w.r.t to the objective function
III. Different weight for each constraint
IV. Different behavior between satisfaction and satisfaction of the constraint
V. Continuously decreasing constraint after satisfaction lead to the search of the minimum value and not just searching for its satisfaction.
VI. Equality constraints ($\alpha_i = \beta_i$) easily imposed

The results of the optimization performed with such a definition is shown in **Figure 5**, from which the improvements are clearly evident.

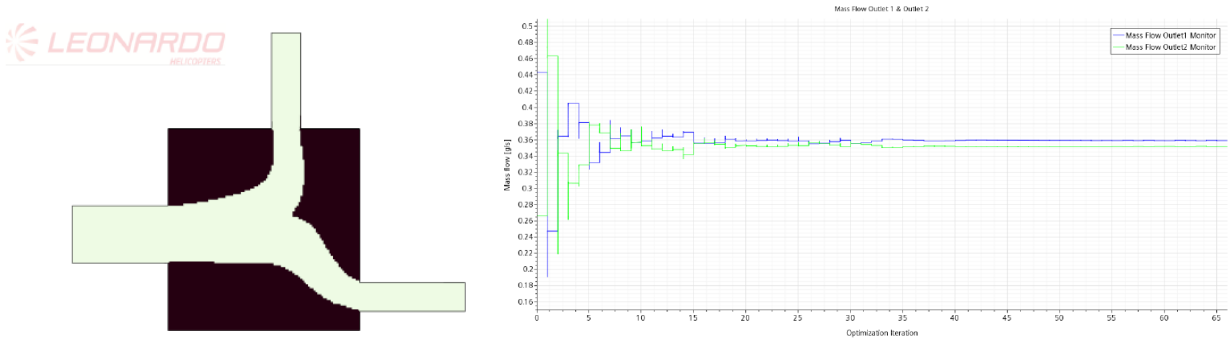

***Figure 5**: Results of the optimization performed with the new normalization. Notice the more stable convergence obtained*

4. Turbulence correction

To validate the new topology obtained and to analyze the goodness of the solid domain simulation through the porous medium, it is necessary to reconstruct the geometry with the optimization and compare the previewed results with the one obtained with the real geometry and the correct near-wall treatment. This comparison showed a non-negligible discrepancy between the two simulations, especially in this case in the pressure field (**Tab. 1**). This error introduced by the Brinkman Penalization Model represents a huge problem for the correct setting of the optimization, especially for the value of the constraints that need to be imposed, and therefore it is fundamental to look for corrections that help in its reduction. Since we are considering an optimization problem, the absolute value of the objective function is not predefined and is not as fundamental as the one of the constraints; the rebuilt geometry can indeed give us its real value. The problem arises when considering the constraints definition: not taking into account such an error in the computation of the physical quantities can lead to an incorrect value of the constraints, which would result in an over-constrained optimization (not capable of improving) or in an under-constrained one (the rebuilt geometry does not satisfy the constraint).

Analyzing the most important physical quantities involved, a major source of error was found in the presence of a non-zero turbulence field within the porous medium. Even tough in the cells characterized with a Material Indicator value different from 1 the momentum is highly reduced (*(Eq. 7*), its value is never absolutely zero but it is some order of magnitude smaller than the velocity scale of the problem. The consequence is that a turbulence may develop or propagate inside the porous medium and influence the behavior of the external fluid (**Figure 6**).

Such a development of turbulence is due to two causes: the lack of a real physical wall with a correct near-wall treatments and a huge shear stress in the interface cells. Together, these lead to a high turbulence production that increases the pressure losses in the system and affect all the solution. A first, simple correction has been here proposed to try to reduce such an error and to improve the solution analysis: the idea behind is based on the general one of the Brinkman Penalization model, i.e. forcing to zero all the turbulence inside the porous medium. A new definition for the turbulence viscosity was therefore introduced:

$$\tilde{\mu}_t = \mu_t \ \ [1 - (1 - \chi)^5] \qquad \textit{(Eq. 11)}$$

Such a definition was made based on two key points:

I. Null turbulence viscosity in cells completely solid ($\chi \approx 0$)
II. No influence on the turbulence field inside the fluid domain ($\tilde{\mu_t} > 0.95\mu|_{\chi>0.5}$)

The effect of the new turbulence viscosity can be seen in **Figure 6** and **Tab. 1**.

Tab. 1: Pressure Drop reduction comparison – Turbulence Correction Effect

Pressure Drop Reduction (w.r.t basic geometry value)			
	Expected value (Brinkman Model)	Obtained Value (Reconstructed geometry)	Expected Value with Turbulence Correction
	-57%	**-81%**	**-69%**

Figure 6: Comparison of the turbulence viscosity field between the basic model (left) and the improved one (right)

5. Model validation – Application on a Real 3D

The improvement introduced in the previous section have been then tested on a real 3D case that however represents a "standard" application case for fluid dynamics topology optimization: generating the best geometry for a ducts system that would reduce the system pressure drop. The base geometry is the one of the Inlet Particle Separator duct with the one of the Starter of the Engine of the NGCTR. The goal of this analysis is to apply the knowledge gained from the 2-D case to a 3-D one, to analyze the possible differences of the TO model, in addition to prove the robustness of such a procedure. An in-depth discussion on the difference between the optimization performed with the basic sensitivity normalization versus the new developed one is presented and the differences are analyzed, along with an analysis of the error introduced by the Brinkman Penalization Model and its reduction with the new turbulent viscosity.

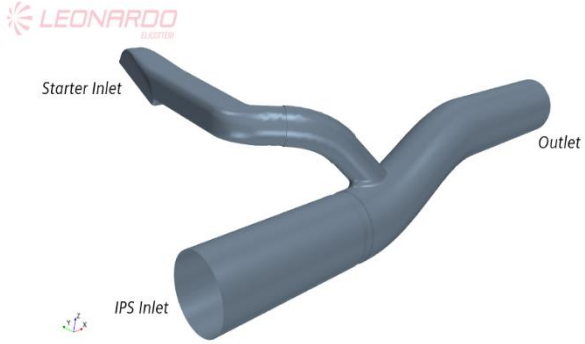

Figure 7: IPS basic geometry

The goal of this optimization was to find the best geometry that can reduce the pressure losses of the system with a maximum on the pressure at the IPS inlet section. In order to keep into account the error introduced by the porous media, the constraint value was increased w.r.t the physical one (from +50% to +100% w.r.t the one of the basic geometry).

Due to external geometry constraints, the topology domain is the same as the actual IPS geometry, with the optimization that could only “dig” into it to improve the objective function but cannot move in the outer directions. The most critical section in which to work was identified (as expected) to be the pipe junction so only those boundaries were characterized as source for the solid domain.

Analyzing the topology obtained with the two different approaches (**Figure 11**), the improvements introduced by the new normalization procedure are clear: not only the topology is more complex but it is also more sensitive to the flow development. According to **Figure 9** and **Figure 8**, it is indeed clear that the effect of the new solid is to help the starter flow in bending and entering the main flow in the smoothest possible way, introducing a sort of "calm room" in which the vertical component of the flow is destroyed: this new feature aims to slow down the flow, which introduces some pressure losses, but that are smaller w.r.t the one that would be introduced with a direct mixing of the two flows. Moreover, two support-like structures have been introduced that helps in recalling the flow from the IPS duct and introducing a rotational component which helps the starter flow in its mixing. All these features ensure a greatest improvement of the objective function with respect to the one obtained with the basic model. Moreover, the turbulence viscosity correction helped in the constraint satisfaction since its previewed value is more coherent with the real one (see **Tab. 2** and **Tab. 3**).

***Figure 11**: Comparison of the final topology between Basic (left) and improved (right) normalization definition*

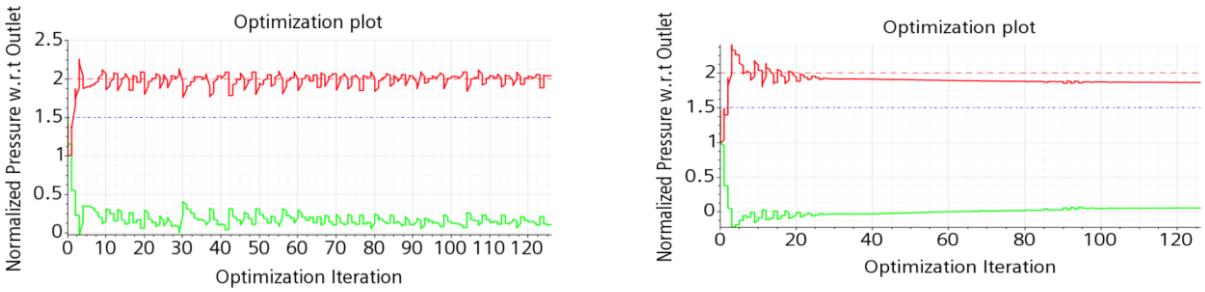

***Figure 10**: Convergence comparison between the basic (left) and new (right) normalization procedure*

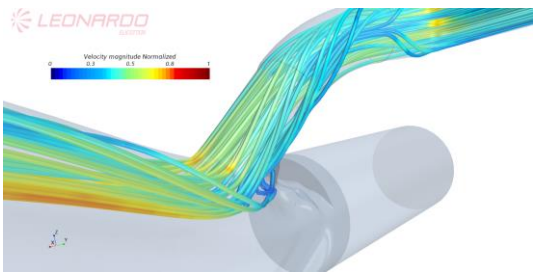

***Figure 9**: Streamline on the Starter duct before the junction (reference geometry). Note the birth of a rotational component in the flow*

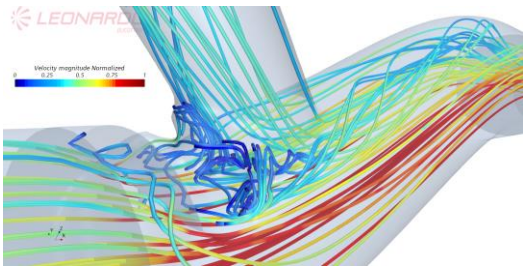

***Figure 8**: Effect of the two support-like structures on the flow behaviour*

Tab. 2: Starter Section Pressure Drop comparison – Basic Model vs Improved Model

Pressure Starter Section (w.r.t basic geometry value)			
Reference Model		Improved Model	
Expected value	Obtained Value	Expected value	Obtained Value
-[70 ; 90]%*	-42%	-90%	**-75%**

* oscillations introduced: full convergence unable to be reached

Tab. 3: IPS Section Pressure Drop comparison – Basic Model vs Improved Model

Pressure IPS Section (w.r.t basic geometry value)			
Reference Model		Improved Model	
Expected value	Obtained Value	Expected value	Obtained Value
+[80 ; 110]%*	+21%	+80%	**+33%**

* oscillations introduced: full convergence unable to be reached

6. NGCTR Primal Exhaust Topology Optimization

The huge improvements experienced with the new procedure introduced in the IPS analysis laid the groundwork for applying such a model to the more complex aerodynamic scenario of the primal exhaust of the NGCTR engine. The greatest difference between this domain and the others here proposed and all the other available in literature (to the authors' best knowledge) resides in the fact that the solid domain here must grow and lie in the middle of the fluid domain and not at its boundaries: the fluid domain is no more included in the new solid, but is the latter that is "bounded" by the fluid. This introduces a new problem in the analysis: the LSF cannot generate solid that is not attached to a physical boundary or to a cell with $\chi < 0.5$, to avoid generation of floating solid inside the domain. A possible solution at this was found by generating a particular initial condition for the material indicator function, that would replicate the actual geometry of the primal exhaust and from which the solid could be introduced in the domain. A side effect of such an initial condition resides on the physical values computed at the end of the "Base Solution": the error introduced by the Brinkman model is yet taken into account, since a porous medium is introduced a priori in the flow field. This makes possible to compare the values of the real actual exhaust with the ones computed with such a particular initial condition, giving a more coherent indication of the error introduced and allowing for a best choice for the constraints' values (cfr. **Tab. 4**).

The main purpose of the primal exhaust of the NGCTR engine is to drive away from the engine itself the hot gasses exiting the turbine, while generating, via the jet pump effect [18], a low pressure region that recalls flow from the engine bay, increasing its speed and therefore its cooling effect. The goal of this optimization is therefore to find the best geometry that can guarantee the following:

I. Maximize the mass flow in the secondary exhaust (MF_{II}) with a maximum backpressure on the turbine outlet section (i.e. minimum backpressure coefficient (C_p^T); or
II. Minimize the backpressure on the turbine outlet section while keeping the mass flow on the secondary exhaust as close as possible to the actual one.

Both the optimization had a constraint on the amount of solid that it could introduce, set equal to the one obtained with the particular initial condition (i.e. same amount of the actual exhaust).

Since no data about the swirl at the turbine outlet was provided, the flow velocity was assumed uniform and normal to the turbine outlet section plane.

***Tab. 4**: Backpressure coefficient values analysis*

C_p^T [-]				
Actual value	Without $\tilde{\mu}$	With $\tilde{\mu}$	Real Constraint*	Imposed constraint
0.42	-0.4	-0.13	**-0.22**	**-1**

* given from the engine installation manual provided by the engine constructor

The analyses performed showed a high level of robustness of the new procedure, since a good guess of the order of magnitude of the sensitivity ratio is enough for having a coherent normalization between the objective function and constraints. However, especially for Case II., some convergence problems have been experienced, with the final topology that is not as defined as the one obtained in Case I., as shown in **Figure 12**. Nevertheless, both the optimizations managed to define a new geometry for the primal exhaust from which to start from a CAD model reconstruction for the real equipment analysis and verification.

***Figure 12**: final topology obtained at the last optimization iteration. Case I (left) showed a good convergence while Case II (right) experienced some oscillations around the optimum*

Analysing the two geometries obtained, it is possible to understand and appreciate the differences in the optimization behaviour: when the objective function and the constraints are switched, the optimization changes completely, and this is correctly felt by the solver with the correct sensitivity ratio. If one of the constraint was too important, the final geometries would have been much more similar between the two optimizations.

***Figure 13**: Reconstructed CAD geometries. Reconstruction process did not take into account for small asymmetries*

Even if for Case I the reconstruction of the topology was straightforward, due to its good and stable convergence, the one of Case II was somehow made considering the general idea given at the last iterations; the resulst obtained are therefore not completely comparable with the previewed one. Nevertheless, both geometries managed to improve the objective function, with a good constraint satisfaction, as reported in **Tab. 5**.

Tab. 5: Final performances – Primal exhaust optimization

MF_{II}*		C_P^T*	
Case I	Case II	Case I	Case II
+15 %	-7%	-0.11	**0.47 (+14.5%)**

* Percentages are referred to the actual geometry's values

In particular, the constraint on the MF_{II} for Case II is not completely satisfied, maybe due to the different geometry obtained with the CAD model w.r.t the one depicted by the optimization.

An in-depth analysis of the flow field depicts the enhancement made by the new topologies into the flow field. In the first case, underneath the horn-like lobed shape, a low-pressure zone in generated thanks to the acceleration of the primal flow, increasing the suction effect on the secondary flow and creating the required space for its acceleration (**Figure 14**), while shrinking the lobed-region entrance section for the remaining flow, channelling it into the main one, which in turn is accelerated by the obstruction generated by the flow deflector at the beginning of the exhaust. The so-defined lobed feature, on the other hand, helps in the mixing of the flows but the lack of a horizontal development of the geometry introduces a huge recirculation zone just after the exhaust itself which leads to a less uniform flow at the outlet section.

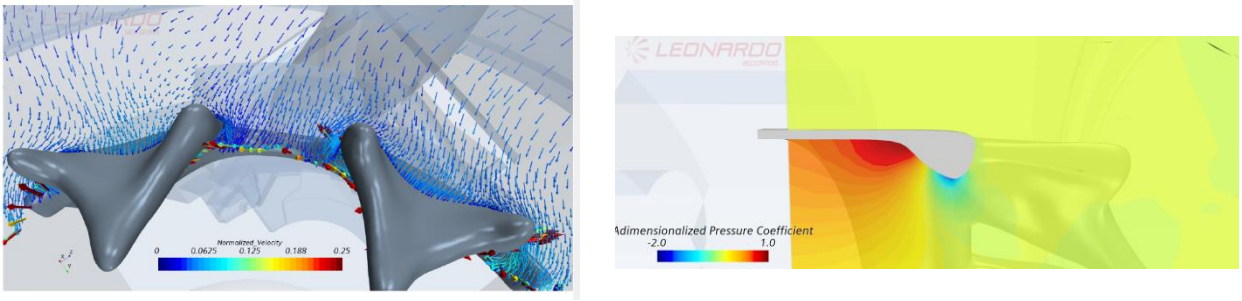

Figure 14: Flow behaviour around the new primal exhaust - Case I

In the second case (**Figure 15**), the vertical development of the lobed-shape is completely deleted and replaced with a purely longitudinal development with the generation of a sort of A-shape. Focusing on the bottom side of these new features. from the edge of the triangular hole starts a groove that develops until the end of the lobed feature and digs into the domed shape. The purpose of triangular hole is channelling the primal flow into the secondary one, reducing the mass flow that undergoes in the lobed region and, therefore, reducing the pressure on the turbine section. The same flow however, filling part of the secondary exhaust, obstructs the suction of the mass flow from the engine bay. The groove, on the other hand, channels part of the primal flow, driving it into the main exhaust section and avoiding (or at least reducing) the separation of the same. Both these two features help in reducing the pressure at the turbine section, while the domed shape seems to reproduce the effect of the horn-like shape obtained in the first case, recalling the secondary flow and improving its mixing with the primal one.

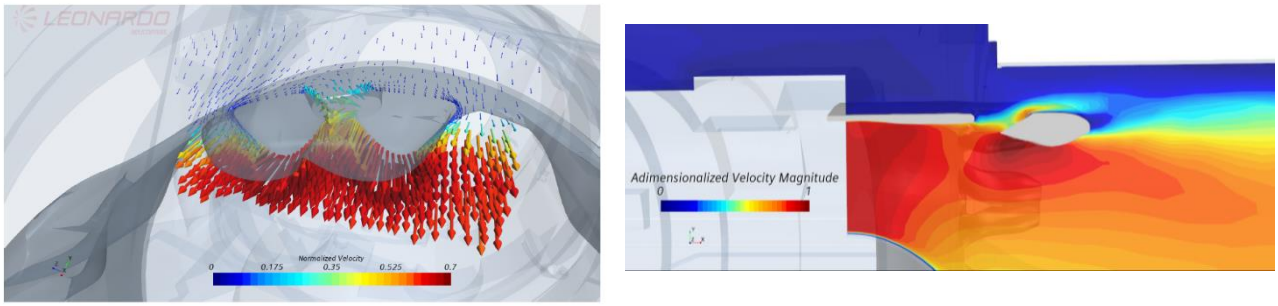

Figure 15: Flow behaviour around the new primal exhaust - Case II

7. Conclusions

In the present paper an analysis of the Adjoin Topology Optimization model with the Brinkman Penalization Model implemented in STAR-CCM+ has been presented. After some considerations about the main characteristics of the optimization itself and its performances, we introduced the new normalization procedure developed to make the optimization more reliable and robust with respect to the physical quantities involved. Moreover, a first correction at the turbulence field generation by the porous medium of the Brinkman Model was introduced and its effect analyzed in the test cases presented. At the end of this paper the optimization was applied to the case of interest, the primal exhaust of the NGCTR engine, with two different goals. Both the optimizations managed to improve the objective function with a good constraint satisfaction and a good and fast convergence at the optimum. Moreover, the introduction of a particular initial condition for the LSF has been reviled a good technique for a first preview of the error introduced in the physical quantities by the porous media. The greatest improvement given from such Initial Condition lies in the possibility introduced in generating solid domain bounded and immersed in the flow domain and not only at its boundaries. Further improvement can and must be made to make Topology Optimization suitable for a huge variety of applications, such the introduction of a correct near-wall treatment for the fluid cells that share a boundary with porous ones and the coupling with a model for the structural and thermal analysis of the solid generated during the optimization itself, in order to perform both a fluid-dynamic and a structural optimization.

Author Contributions: All authors have read and agreed to the published version of the manuscript.

Funding: "This research has received funding from the Clean Sky 2 Joint Undertaking (JU) under grant agreement No 945542. The JU receives support from the European Union's Horizon 2020 research and innovation programme and the Clean Sky 2 JU members other than the Union."

Conflicts of Interest: The authors declare no conflict of interest.

References

1. M.P. Bendsøe and N Kikuchi. "Generating optimal topologies in structural design using a homogenization method". (1988). https://doi.org/10.1016/0045-7825(88)90086-2.
2. Casper Schousboe Andreasen Joe Alexandersen. "A Review of Topology Optimisation for Fluid-Based Problems". (2020). doi: 10.3390/fluids5010029
3. AIA, "Additive Manufacturing "Best Practices". https://www.aia-aerospace.org/wp-content/uploads/2020/02/AIA-Additive-Manufacturing-Best-Practices-Report-Final-Feb2020.pdf
4. Marika Belardo et. Al, "Safety of Flight approach for Fuel tanks ALM flanges for Tiltrotor Application", (2021)
5. Ramana V Grandhi. "A survey of structural and multidisciplinary continuum topology optimization: post 2000". In: (2014). doi: 10.1007/s00158-013-0956-z.
6. Siemens STAR CCM+. url: https://www.plm.automation.siemens.com/global/it/products/simcenter/STAR-CCM.html.
7. J. Petersson T. Borrvall. "Topology optimization of fluids in Stokes flow". (2003). doi: 10.1002/fld.426.
8. Clean Sky Joint Undertaking. url: https://www.cleansky.eu/. (Accessed:9/12/2020).
9. Leonardo Helicopters. url: https://www.leonardocompany.com/it/innovation/future-programmes/next-generation-civil-tiltrotor-ngctr. (Accessed: 9/12/2020).
10. Andreas Wiegmann J.A.Sethian. "Structural Boundary Design via Level Set and Immersed Interface Methods". In: (2000). doi: https://www.sciencedirect. com/science/article/pii/S0021999100965811
11. Wang et al. "A level set method for structural topology optimization". (2003). doi: 10.1016/S0045-7825(02)00559-5.
12. Sebastian Kreissl · Kurt Maute. "Levelset based fluid topology optimization using the extended finite element method". (2012). doi: 10.1007/s00158-012-0782-8.
13. Subhayan De et al. "Topology Optimization under Uncertainty using a Stochastic Gradient-based Approach". In: Structural and Multidisciplinary Optimization (2020). doi: 10.1007/s00158-020-02599-z.
14. Jimmy Ba Diederik P. Kingma. "Adam: A Method for Stochastic Optimization". (2014).
15. Philippe Angot. "A penalization method to take into account obstacles in incompressible viscous flows". In: Numerische Mathematik (1999). doi: 10.1007/s002110050401
16. Sebastian Kreissl, Georg Pingen, and Kurt Maute. "Topology optimization for unsteady flow". In: International Journal for Numerical Methods in Engineering (2011). doi: https://doi.org/10.1002/nme.3151.
17. Sebastian Kreissl, Georg Pingen, and Kurt Maute. "An explicit level set approach for generalized shape optimization of fluids with the lattice Boltzmann method". In: International Journal for Numerical Methods in Fluids (2011). doi: https://doi.org/10.1002/fld.2193.
18. Na T.Y. Cunningham R.G. Hansen A.G. "Jet pump cavitation". (1970). doi: 10.1115/1.3425040.